

Stay Hydrated! Impact of Solvation Phenomena on the CO₂ Reduction Reaction at Pb(100) and Ag(100) surfaces

Oskar Cheong,^[a, b, c] Thomas Bornhake,^[a, c] Xinwei Zhu,^[a, b, c] and Michael H. Eikerling^{*[a, b, c]}

Herein, a comprehensive computational study of the impact of solvation on the reduction reaction of CO₂ to formic acid (HCOOH) and carbon monoxide on Pb(100) and Ag(100) surfaces is presented. Results further the understanding of how solvation phenomena influence the adsorption energies of reaction intermediates. We applied an explicit solvation scheme harnessing a combined density functional theory (DFT)/microkinetic modeling approach for the CO₂ reduction reaction. This approach reveals high selectivities for CO formation at Ag and

HCOOH formation on Pb, resolving the prior disparity between ab initio calculations and experimental observations. Furthermore, the detailed analysis of adsorption energies of relevant reaction intermediates shows that the total number of hydrogen bonds formed by HCOO plays a primary role for the adsorption strength of intermediates and the electrocatalytic activity. Results emphasize the importance of explicit solvation for adsorption and electrochemical reaction phenomena on metal surfaces.

Introduction

For realistic atomistic simulations of electrochemical reactions at electrode/electrolyte interfaces, it is of utmost importance to account for solvation phenomena. These phenomena can have a significant impact on the energetics of different reaction pathways.^[1–4] Different approaches to treat solvation on metal surfaces were considered in the past, ranging from implicit over explicit to hybrid solvation models.^[1–16] Implicit solvation models treat the solvent as a polarizable continuum and thereby minimize computational cost. However, recent studies have shown that H-bonding in the vicinity of solvated reaction intermediates plays a crucial role in the stabilization of adsorbates.^[2,7,14] Heenen et al.^[7] compared adsorption energies of several adsorbates on different metal surfaces obtained using an implicit treatment of solvation effects with adsorption energies calculated from ab initio molecular dynamics (AIMD) simulations. They found that the adsorption energies derived by the continuum solvation method and AIMD simulations differed by up to 0.6 eV. Furthermore, they found no significant

improvement of computed adsorption energies compared to vacuum calculations when the implicit solvation scheme was applied.

Explicit solvation models can be divided into static and dynamic approaches. Within the realm of static water approaches, the number of water molecules considered explicitly ranges from several molecules^[2,13,14,17] to static ice-like water bilayers.^[17–19] Di Liberto et al.^[17] have demonstrated that the presence of a few explicit water molecules is sufficient to mimic the adsorption characteristics of oxygenates on Pt(111) in a water bilayer environment. An alternative microsolvation approach, proposed by Rendon-Calle et al.,^[11] involves quantifying the required number of water molecules in the first solvation shell of adsorbates by taking into account the additional stabilization of hydrogen bonding interactions with the adsorbate. This approach predicted onset potentials of CO₂ reduction reactions to CO, CH₄, and CH₃OH on Cu, Ag, Au, and Zn, in reasonable agreement with experimental values. However, the main challenge of static microsolvation approaches is the difficulty identifying a representative structure from the vast number of configurations possible within the adsorbate-solvent system as well as the negligence of solvation effects that extend beyond the first solvation shell of the adsorbate. Even if we adapt the convenient static hexagonal ice-like water layer, the transferability of these static structures becomes more difficult when accounting for surface facets other than (111) and metal lattice parameters that deviate from those of the frequently investigated Cu or Pt.


Explicit dynamic approaches such as classical MD (CMD) and AIMD can overcome the lack of sufficient statistical sampling of relevant configurations. However, AIMD simulations lack the computational efficiency to sample a sufficient number of configurations over a sufficiently long time scale.^[20–22] On the other hand, CMD simulations of water structures on metal surfaces rely on the accurate parametrization of force fields.^[22–24] Hybrid approaches such as the quantum-mechanical/molecular mechanics (QM/MM) method, in which surface-adsorbate

[a] O. Cheong, T. Bornhake, X. Zhu, Prof. Dr. M. H. Eikerling
Institute of Energy and Climate Research (IEK-13), Forschungszentrum
Jülich, Wilhelm-Johnen-Straße, 52425 Jülich, Germany
E-mail: m.eikerling@fz-juelich.de

[b] O. Cheong, X. Zhu, Prof. Dr. M. H. Eikerling
Chair of Theory and Computation of Energy Materials, Faculty of
Geosciences and Materials Engineering, RWTH Aachen University,
Intzestrasse 5, 52072 Aachen, Germany

[c] O. Cheong, T. Bornhake, X. Zhu, Prof. Dr. M. H. Eikerling
JARA Energy & Center for Simulation and Data Science (CSD), 52425 Jülich,
Germany

 Supporting information for this article is available on the WWW under
<https://doi.org/10.1002/cssc.202300885>

 © 2023 The Authors. ChemSusChem published by Wiley-VCH GmbH. This is
an open access article under the terms of the Creative Commons Attribution
Non-Commercial NoDerivs License, which permits use and distribution in
any medium, provided the original work is properly cited, the use is non-
commercial and no modifications or adaptations are made.

interactions are described at the quantum mechanical level and adsorbate-solvent interactions are modeled using classical molecular mechanics, have yielded promising results for the calculation of adsorption energies of benzene and phenol at the Pt(111)/water interface, for which experimental data are available to compare with.^[10] As this approach also relies on the force field parameters for adsorbate-solvent and solvent-surface interactions, it can be stated that while a lot of research works on different solvation approaches at metal surfaces were published, there is still no consistent approach to treating solvation of adsorbates on metal surfaces. Specifically, there is still no clear guidance on how to account for explicit solvation in the CO₂ reduction reaction.

In the latter context, Pb is a promising electrocatalyst for CO₂ reduction^[25–28] to formic acid (HCOOH), which has many uses in the fields of fuel cells, pharmaceuticals and crop protection,^[29–31] while CO₂ reduction at Ag mainly produces CO, which serves as an industrial feedstock for a wide range of chemicals.^[32] Whereas it has been experimentally shown that CO₂ reduction generates mostly HCOOH on Pb catalyst and CO on Ag catalyst,^[3,25,33,34] these experimental observations have so far not been demonstrated conclusively with ab initio simulations.^[35] DFT calculations in vacuo allow for fast screening of selective catalytic materials.^[34–37] However, in the case of CO₂ reduction to HCOOH or CO, solely evaluating the adsorption energies of reaction intermediates in vacuo can be insufficient for correctly predicting product selectivities. In particular, adsorption energy calculations of Yoo et al.^[35] have suggested that HCOOH is the main product for CO₂ reduction on both Ag and Pb surfaces, contradicting experimental results. In recent years, there have been several attempts to resolve this Ag/Pb selectivity issue.^[38–41] Morrison et al.^[38] tried to explain the selectivity for CO formation on Ag and HCOOH formation on Pb by coverage-dependent adsorption energies of HCOO and COOH intermediates. Other computational works based on DFT found CO to be the main product during CO₂ reduction on Ag. These conclusions were reached with different reasoning: (1) based on the inclusion of lateral interactions of reaction intermediates,^[39] (2) based on the discovery of new reaction intermediates^[40] and (3) based on the incorporation of one extra solvent molecule.^[41] However, it remains unclear whether the aforementioned explanations can be extended to HCOOH-selective catalytic materials such as Pb. We thus expect that further refined consideration of solvation effects for the CO₂ reduction reaction on both Pb(100) and Ag(100) surfaces could improve the consistency with experimental findings.

Realizing the lack of understanding of solvation effects during reaction energy calculations, we provide comprehensive insights into how different solvation approaches affect adsorption energies of certain reaction intermediates as well the overall CO₂ reduction reaction pathway towards HCOOH or CO on Pb(100) and Ag(100) surfaces. We have combined DFT calculations with microkinetic modeling to re-evaluate product selectivities of the CO₂ reduction reaction on Pb(100) or Ag(100) surfaces. Based on these results, we follow up with an examination of various critical aspects of the explicit solvation approach by carrying out an uncertainty analysis for the explicit

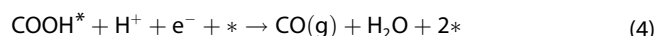
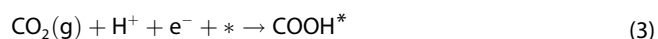
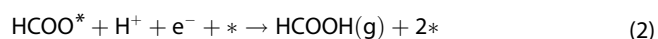
solvation effect of reaction intermediates HCOO or COOH on Pb(100). Additionally, we explore crucial properties that affect the adsorption energy of these reaction intermediates.

Results and Discussion

Solvation effect on CO₂ reduction reaction towards HCOOH or CO on Pb(100) surface

To show the importance of solvation when evaluating electrochemical reactions, we have investigated the effect of explicit and implicit solvation on the CO₂ reduction reaction at the Pb(100) surface. CO₂ reduction on Pb(100) (also on Ag(100)) proceeds via two major pathways. Following the first pathway, CO₂ is transformed to HCOOH via the HCOO* reaction intermediate (Eqs. (1) and (2)). The second pathway proceeds to CO and H₂O products via the COOH* reaction intermediate (Eqs. (3) and (4)).

The considered reaction pathways to CO and HCOOH are given by



where $*$ indicates a free adsorption site and adsorbed intermediates are indicated with $*$.

Reaction energies for the first CO₂ reduction reaction step for the vacuum case and different solvation methods are summarized in Table 1. For the explicit solvation case, 12 explicit H₂O molecules were used, equivalent to one water layer.^[42] The reaction or adsorption energy for the first reaction step of CO₂ to HCOO* or COOH*, Equations (1) and (3), is calculated using the relation

$$E_{\text{ads}} = E_{\text{HCOO/COOH+surface}} - E_{\text{surface}} - E_{\text{CO}_2} - 0.5 * E_{\text{H}_2} \quad (5)$$

where $E_{\text{HCOO/COOH+surface}}$, E_{surface} , E_{CO_2} , and E_{H_2} correspond to the energy of adsorbed HCOO* or COOH* on the Pb(100) surface, the energy of the bare Pb(100) surface and the energies of

Table 1. Adsorption energy of HCOO*, $E_{\text{ads,HCOO}}$ and COOH*, $E_{\text{ads,COOH}}$ on the Pb(100) surface for the vacuum case and the different solvation scenarios, encompassing implicit, explicit and hybrid solvation. 12 explicit H₂O molecules are considered for the explicit solvation case and the hybrid solvation case.

Method	$E_{\text{ads,HCOO}}$ [eV]	$E_{\text{ads,COOH}}$ [eV]
vacuum	−0.37	0.75
implicit	−0.57	0.56
explicit	−1.11	0.53
hybrid	−1.18	0.48

isolated gas-phase species, CO_2 and H_2 , respectively. In this study, the terms reaction energy and adsorption energy are used interchangeably, conveying the same underlying concept. According to the CHE method,^[43] the free energy of H_2 instead of the free energies of protons and electrons is employed. In solvated environment, instead of the energies of adsorbed HCOO^* or COOH^* , $E_{\text{HCOO/COOH} + \text{surface}}$ and of the bare $\text{Pb}(100)$ surface, E_{surface} the energies of the solvated adsorbed HCOO^* and COOH^* on the $\text{Pb}(100)$ surface, $E_{\text{HCOO/COOH} + \text{surface} + n\text{H}_2\text{O}}$ and of the solvated $\text{Pb}(100)$ surface, $E_{\text{surface} + n\text{H}_2\text{O}}$ are included, with $n\text{H}_2\text{O}$ representing the number of explicit water molecules. In the Theoretical Section a more detailed explanation of the initial configuration of water molecules considered in the explicit solvation case is provided.

Similar calculations were performed in our previous study,^[44] where VASP^[45–47] and VASPsol^[48,49] software packages were used to perform DFT calculations in vacuum and in solvation. As observed in the previous study,^[44] applying implicit solvation stabilizes reaction energies of HCOO^* and COOH^* by around 0.2 eV relative to the vacuum case. The difference between these reaction energies remains the same as in the vacuum case. Implicit solvation stabilizes these intermediates by an equal amount without incurring a change in their configuration relative to the vacuum case, as shown in Figure S1 of the Supporting Information. Explicit solvation in the case of 12 explicit water molecules results in a different picture. HCOO^* is stabilized by 0.74 eV, whereas COOH^* is stabilized by only 0.22 eV in the explicit solvation environment. Overall, these results agree with our previous findings.^[44] In addition to these findings, we explain the greater stabilization of HCOO^* compared to COOH^* with the fact that explicit water molecules have a significant impact on the orientation of HCOO^* relative to the surface, as illustrated in Figure 1. HCOO^* changes from perpendicular orientation towards the surface for vacuum and implicit solvation cases to parallel orientation for the explicit solvation case. COOH^* on the other hand remains in perpendicular orientation for both cases. In addition, HCOO^* undergoes H-bonding with four neighboring water molecules, while COOH^* is only H bonded to three neighboring water molecules. Lastly, we have found that the hybrid approach, i.e., adding implicit solvation on top of explicit solvation, incurs only a

minor change in the reaction energies of the explicit solvation case, underlining the importance of including explicit water molecules for reaction pathway calculations.

In order to assess the results of our DFT calculations, Table 2 compares the onset potential for HCOOH formation, identified as the minimum potential required to initiate the electrochemical reaction, in the various computational setups used by us, with the experimental HCOOH onset potential. While we observe a significant discrepancy between the experimental value and the computed values for the vacuum and implicit solvation cases, experimental and computed values are close for the explicit solvation case and even closer for the hybrid solvation case.

Realizing the importance of computing solvent effects with explicit water molecules, we have further evaluated the effect of the adsorption energies of both HCOO^* and COOH^* intermediates by systematically increasing the number of explicit water molecules. This gives us a more advanced path towards understanding how many explicit solvent molecules are needed to capture water-adsorbate interactions. Figure 2a illustrates the adsorption energy of HCOO^* with increasing number of up to 12 explicit water molecules (indicated in blue). While we initially calculated the adsorption energy of HCOO^* to be around -0.7 eV for 1–2 explicit water molecules, the adsorption energy of HCOO^* further stabilizes to -0.95 eV for 3–7 explicit water molecules and even up to -1.42 eV for 8–12 explicit water molecules.

This stabilization of HCOO^* with increasing number of water molecules can be rationalized with the increasing number of H-bonds between HCOO^* and water molecules as well as the transformation of the HCOO^* -water system from a cluster for lower number of H_2O molecules to a connected water layer for higher number of H_2O molecules, due to the increased number of H-bonds (see Figure S2 in the Supporting Information). Thus, for the specific case considered here, at least eight explicit water molecules are needed to capture the impact of explicit solvation on the adsorption energy of solvated HCOO^* . In general, to find the sufficient number of explicit water molecules, one has to ensure that the number of hydrogen bonds in the water-adsorbate system is saturated. For HCOO^* it is four hydrogen bonds, with two hydrogen bonds between each oxygen of HCOO^* and its surrounding water molecules. In the case of COOH^* (Figure 2b), the trend is not as clear as for HCOO^* . The adsorption energy of COOH^* does not vary

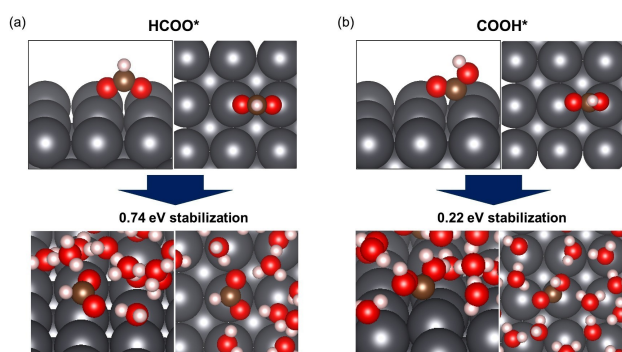


Figure 1. Illustration of configurational change from vacuum to explicit solvation for (a) HCOO^* adsorbate and (b) COOH^* adsorbate on $\text{Pb}(100)$ surface.

Table 2. Onset potential (vs. RHE at $\text{pH}=0$) for HCOOH formation on Pb for the vacuum case, the different solvation scenarios, encompassing implicit, explicit, and hybrid solvation and the experimental case. The experimental onset potential for HCOOH formation is taken from Ref. [3].

Method	HCOOH onset potential [V]
vacuum	-0.24
implicit	-0.44
explicit	-0.98
hybrid	-1.05
experimental	-1.08

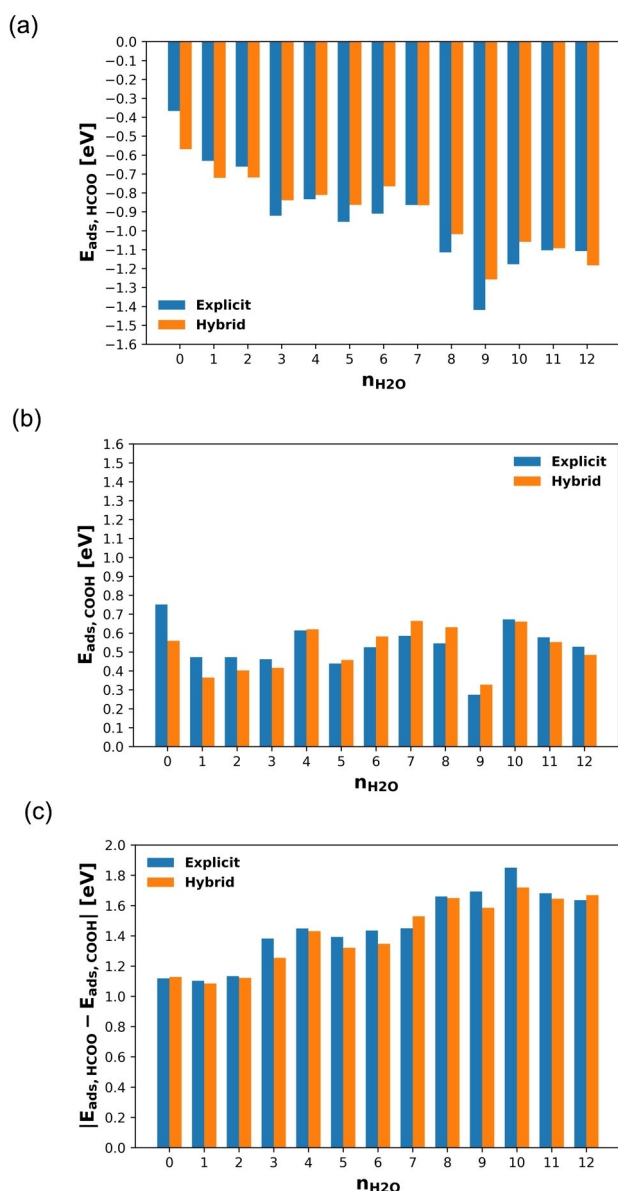


Figure 2. Adsorption energy of (a) $HCOO^*$ and (b) $COOH^*$ on Pb(100) surface and (c) the adsorption energy difference of $HCOO^*$ and $COOH^*$ using explicit and hybrid solvation methods, with the number of explicit H_2O molecules, n_{H_2O} , ranging from 0 to 12. The hybrid case at 0 H_2O shows the purely implicit solvation case.

significantly with increasing number of explicit water molecules. The $COOH^*$ adsorption energy was determined to be 0.47 eV for the case of one explicit H_2O molecule, and it remained nearly the same, 0.53 eV, for the case of 12 explicit H_2O molecules. As mentioned earlier, the $COOH^*$ reaction intermediate forms fewer hydrogen bonds with surrounding water molecules and therefore maintains a relatively unchanged configuration compared to vacuum or implicit solvation cases. This observation can be explained with the adsorbate-water interaction being weaker for $COOH^*$ than for $HCOO^*$.

Figure 2c shows the difference of adsorption energies between $HCOO^*$ and $COOH^*$, $|E_{ads, HCOO} - E_{ads, COOH}|$, with increasing n_{H_2O} . The difference increases from 1.12 eV in vacuo up to 1.85 eV in the explicit solvation environment, primarily due to the significant increase of $E_{ads, HCOO}$ for explicit solvation. As can be deduced from the direct comparison of results obtained in explicit and hybrid solvation schemes (denoted here as "hybrid"), adding additional implicit solvation does not alter the reaction energies significantly.

We have also performed additional adsorption energy calculations with D3 corrections to assess the need of including dispersion effects in our work. Table 3 shows the $HCOO^*$ adsorption energy, $E_{ads, HCOO}$, $COOH^*$ adsorption energy, $E_{ads, COOH}$, and the adsorption energy differences of $HCOO^*$ and $COOH^*$, $|E_{ads, HCOO} - E_{ads, COOH}|$, for 0, 1, 6, 11, and 12 explicit water molecules on the Pb(100) surface with and without dispersion D3 corrections. Although the addition of dispersion corrections stabilizes both reaction intermediates, viz. $HCOO^*$ and $COOH^*$, the resulting adsorption energy differences of $HCOO^*$ and $COOH^*$, which play a crucial role in determining the selectivity of the considered reaction pathways, differ less than 0.05 eV compared to the case without dispersion corrections for all cases. Due to the small impact of dispersion corrections for our system, we have not included dispersion corrections in further calculations.

Reaction energy pathways for CO_2 reduction reaction on Pb(100) and Ag(100) surfaces

DFT calculations

In this section, we evaluate the effect of explicit solvation on reaction energies and selectivities of CO_2 towards formation of

Table 3. $HCOO^*$ adsorption energy, $E_{ads, HCOO}$, $COOH^*$ adsorption energy, $E_{ads, COOH}$, and adsorption energy difference of $HCOO^*$ and $COOH^*$, $|E_{ads, HCOO} - E_{ads, COOH}|$, for 0, 1, 6, 11, and 12 explicit water molecules on Pb(100) surface with and without dispersion D3 corrections. Results obtained without dispersion corrections are also illustrated in Figure 2.

Number of H_2O molecules	$E_{ads, HCOO}$ [eV]		$E_{ads, COOH}$ [eV]		$ E_{ads, HCOO} - E_{ads, COOH} $ [eV]	
	PBE	PBE + D3	PBE	PBE + D3	PBE	PBE + D3
0	-0.37	-0.51	0.75	0.61	1.12	1.11
1	-0.63	-0.81	0.47	0.32	1.10	1.14
6	-0.91	-1.22	0.53	0.23	1.43	1.45
11	-1.10	-1.30	0.58	0.36	1.68	1.66
12	-1.11	-1.24	0.53	0.40	1.64	1.64

HCOOH and CO on both Pb(100) and Ag(100) surfaces compared to the vacuum case. The reaction pathways towards CO and HCOOH were discussed in the previous section, where the HCOO* pathway (Eqs. (1) and (2)) represents CO₂ reduction to HCOOH via HCOO* and the COOH* pathway (Eqs. (3) and (4)) represents CO₂ reduction to CO via COOH*. For simulations in the explicit solvation scheme, we have incorporated 12 explicit water molecules at the Pb(100) surface and 8 explicit water molecules at the Ag(100) surface, which are equivalent to the formation of one complete water layer at each surface, respectively.^[42,50] In order to identify the transition states and activation barriers between reaction steps, we have utilized the climbing image nudged elastic band (CINEB) method.^[51]

Figure 3 illustrates HCOO* and COOH* reaction energy pathways at both Ag(100) and Pb(100) in vacuo. For the first reduction step, CO₂ favours the HCOO* pathway towards the HCOO* intermediate on both Ag and Pb with activation energies, $G_{a,HCOO^*}$ of 0.64 eV and 0.29 eV, respectively; the first step of the COOH* pathway exhibits activation energies, $G_{a,COOH^*}$ of 1.76 eV and 1.62 eV, respectively. The stronger preference for the HCOO* pathway and thus the reaction towards HCOOH as a product is supported by HCOO* being more stable than COOH* by 1.05 eV and 1.19 eV on the Ag and Pb surfaces, respectively. Thus, reaction energy pathway calculations for the vacuum case indicate HCOOH as the main product of CO₂ reduction on both metal catalysts, in contradiction to experimental observations.^[3,25,33,34] Similar to the vacuum case, we obtain a significantly higher activation barrier for the formation of COOH* compared to the formation of HCOO* on the Ag surface using implicit solvation (Figure S3 in Supporting Information). Consequently, reaction energy calculations with implicit solva-

tion reaffirm HCOOH as the primary product on Ag, consistent with the observations made in the vacuum case.

In order to determine whether explicit solvation effects can resolve this issue, we have repeated reaction energy pathway calculations, but now with the addition of explicit solvation (Figure 4). In the explicit solvation case, the protons required for hydrogenation reactions, e.g., in $\text{CO}_2 + \text{H}^+ + \text{e}^- \rightarrow \text{HCOO}^*$ or COOH^* , originate from hydronium ions (H_3O^+) in water, employed in previous computational works to elucidate the mechanism of the CO₂ reduction reaction in solvation environment.^[4,52] More details on the H_3O^+ -hydrogenation mechanism are given in Figure S4 of the Supporting Information.

In contrast to the the vacuum case, including explicit water molecules in simulations allows for explicit water-CO₂ interactions to be accounted for. By incorporating explicit water-CO₂ interactions, we are capable of modeling the CO₂ transformation from linear to bent structure, which is a vital initial step of the CO₂ reduction reaction.^[53] The transformation of CO₂ in linear configuration to CO₂ in bent configuration requires 1.21 eV at the Pb(100) surface, while <0.60 eV are needed at the Ag(100) surface. This observation aligns with experimental results, where Ag was observed to be more "CO₂-active" than Pb.^[3,54,55] In addition, under explicit solvation conditions, the activation energy required for the transformation of CO₂ to HCOO* and COOH* is lower for HCOO* at Pb, leading to HCOOH as the product. Conversely, COOH* is more favourable at Ag leading to the production of CO. This finding agrees well

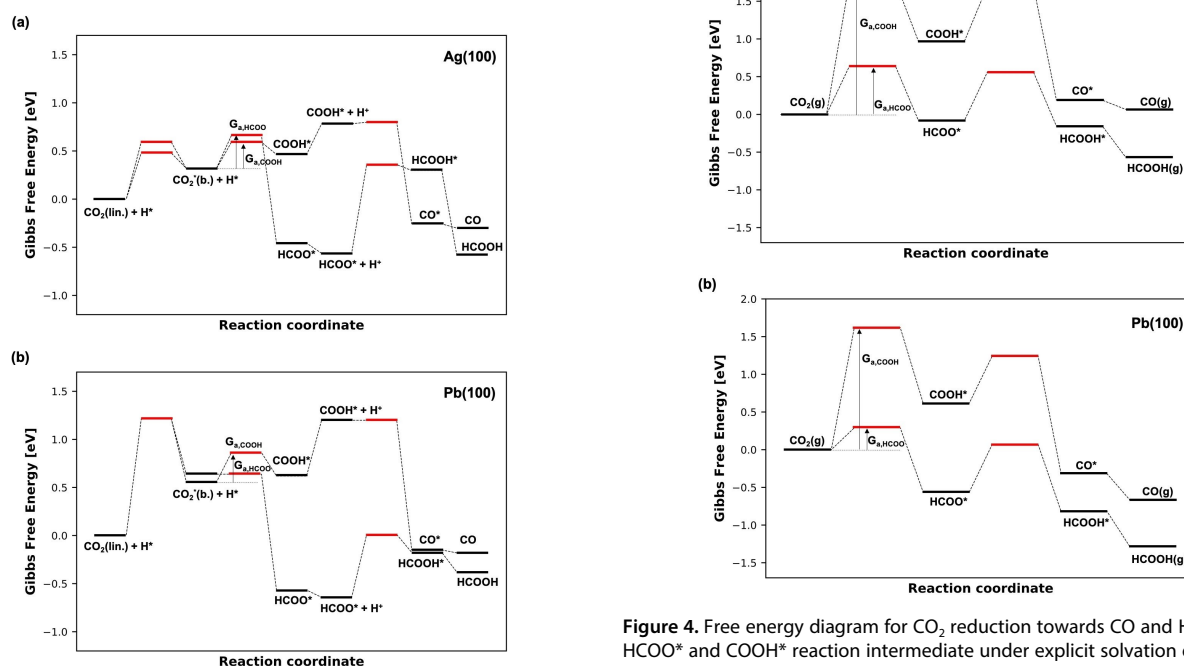


Figure 3. Free energy diagram for CO₂ reduction towards CO and HCOOH via HCOO* and COOH* reaction intermediate under vacuum environment on (a) Ag(100) surface and (b) Pb(100) surface. Red lines and asterisk represent activation barrier (G_a) and adsorbed solute state, respectively.

Figure 4. Free energy diagram for CO₂ reduction towards CO and HCOOH via HCOO* and COOH* reaction intermediate under explicit solvation environment on (a) Ag(100) surface and (b) Pb(100) surface. Asterisk, lin. and b. represent transition states, adsorbed solute state, linear configuration and bent configuration, respectively. H* represents the presence of H_3O^+ ion in the system, which is used for activation barrier calculation (indicated in red) of hydrogenation reactions.

with experimental observations. Simulations under vacuum and implicit solvation conditions on the other hand predict HCOOH as the preferred product at both surfaces. Regarding the reaction step from HCOO* to HCOOH, we observe the same activation energy of 0.64 eV on both Pb and Ag surfaces under vacuum conditions. In the explicit solvation case, the activation energy remains similar for Pb (0.65 eV), while it increases to 0.92 eV for Ag, limiting the further reaction to HCOOH product.

Thermodynamic and kinetic analysis

To further analyze the kinetics of the process, we have employed a microkinetic model to assess the product selectivity at both Ag and Pb surfaces using our calculated reaction and activation energies under vacuum environment and solvated environment. Microkinetic modeling has previously shown to be an essential tool for quantitative analysis of multiple-pathway reactions.^[56–58] In the vacuum case, the microkinetic model results in selectivities of $s_{\text{CO}} \approx 0$ and $s_{\text{HCOOH}} \approx 1$ at both Ag(100) and Pb(100) surfaces, which contradicts experimental observations. The numerical results show that both Ag(100) and Pb(100) prefer the HCOOH pathway in vacuo since the coverage of HCOO* is much higher than that of COOH*, resulting in the high preference for the production of HCOOH. Also for the implicit solvation case, microkinetic modeling results in selectivities of $s_{\text{CO}} \approx 0$ and $s_{\text{HCOOH}} \approx 1$ at the Ag(100) surface, consistent with the findings of the vacuum case. Similar to the vacuum case, it fails to predict HCOOH as the primary product at the Ag(100) surface.

For the explicit solvation case, we follow the same above procedure to obtain HCOOH and CO product selectivities from our microkinetic model. Details on the reaction mechanism and the rate equations of the microkinetic model in the explicit solvation case are given in the Supporting Information.

Given the reaction energies and activation barriers in Figure 4, we obtain $s_{\text{CO}} \approx 1$ and $s_{\text{HCOOH}} \approx 0$ for Ag(100) and $s_{\text{CO}} \approx 0$ and $s_{\text{HCOOH}} \approx 1$ for Pb(100), which matches experimental results. In solvated explicit environment, the coverage of HCOO* is also higher than that of COOH* on both Ag(100) and Pb(100). However, the desorption barrier of HCOO* to HCOOH on Ag(100), as shown in Figure 4, is too high to favor the HCOO* pathway, leading to a preference for the CO pathway, whereas the desorption barrier of HCOO* on Pb(100) is moderate, enabling a preferential pathway for HCOOH.

It should be noted here that our DFT analysis and microkinetic modelling are relevant at 0 V vs. RHE. For the specific case considered in this work, microkinetic modeling under more negative potentials would be more accurate, since the theoretical equilibrium potentials for HCOOH and CO are -0.17 V vs. RHE and -0.12 V vs. RHE, respectively.^[35] For consideration of other electrochemical conditions (i.e., different electrode potential), potential-dependent activation barriers from DFT calculation would be required, which goes beyond the scope of this work. During microkinetic modeling, we make a distinction in the proton source between the vacuum case and the explicit solvation case. In the explicit solvation case, the

proton originates from the H_3O^+ -ion present in water, as elaborated in the previous section. In the vacuum phase, the proton originates from hydrogen adsorbed on the metal surface, formed via the Tafel reaction.

Explicit solvation uncertainty analysis of HCOO* and COOH* adsorption energy

While we have shown in the previous section that explicit solvation has a significant impact on both adsorption energies of HCOO* and COOH* reaction intermediates and product selectivities on Pb(100) and Ag(100) surfaces, a sufficient sampling of explicit water configurations is required to correctly assess the uncertainty of the solvated adsorption energy of reaction intermediates. In this section we used a combined MD/DFT approach to analyze the uncertainty of HCOO* and COOH* adsorption energies on the Pb(100) surface in the presence of n ($n=6, 12$) explicit water molecules. Similar CMD/DFT procedures were proposed in the past to study solvent effects for methanol electrooxidation on gold^[13] as well as important reaction species for ammonia synthesis on Pt.^[59] We initially ran a 10 ns MD trajectory of 95 explicit water molecules on the Pb surface, equivalent to a water density of 1 g L^{-1} . We then picked out 19 different configurations equally spaced over this time span (1 ns, 1.5 ns, 2 ns ..., 10 ns), removed all explicit water molecules except for 6 and 12 explicit water molecules closest to the Pb surface and optimized the obtained configurations using DFT to obtain a range of adsorption energies for HCOO* and COOH*. An illustration of the combined MD/DFT procedure is shown in Figure S5 of the Supporting Information. The purpose of this combined MD/DFT procedure is to quantify the adsorption energy range of HCOO* and COOH* in explicit solvation and to assess the commonly overlooked uncertainty range that arises from analyzing stationary water-adsorbate configurations. Given that water structure equilibration could typically take several hundreds of picoseconds,^[22] using AIMD for this task would be computationally too expensive. Conversely, classical molecular dynamics (CMD) requires a suitable force field to obtain energies that closely resemble those obtained through quantum mechanical methods. Thus, with the combined MD/DFT method, water structures are equilibrated using CMD followed by the DFT optimization of the structures to obtain more accurate energies.

In Table 4, we have summarized the standard deviations (SD) for calculating solvated adsorption energies for both reaction intermediates HCOO* and COOH* on the Pb(100) surface in the explicit solvation environment.

Regarding the adsorption energy of HCOO*, it is evident that increasing the number of explicit water molecules from 6 H_2O to 12 H_2O increases the standard deviation (SD) by 0.07 eV and the minimum-maximum range by more than 0.25 eV, indicating a growing degree of uncertainty and sensitivity with increasing number of H_2O molecules. While the HCOO* adsorption energy with 6 water molecules ranges from around -0.60 eV to -1.13 eV, for 12 water molecules the HCOO* adsorption energy ranges from -0.48 eV to -1.28 eV. In the

Table 4. Statistical mean, minimum (Min), maximum (Max) and standard deviation of the mean value (SD) of HCOO* adsorption energies, $E_{\text{ads,HCOO}^*}$ and COOH* adsorption energies, $E_{\text{ads,COOH}^*}$ on Pb(100) surface in the presence of 6 and 12 explicit water molecules from the combined MD/DFT method. The sample size is $n = 19$.

Pb(100) variables	$E_{\text{ads,HCOO}^*}$ [eV]		$E_{\text{ads,COOH}^*}$ [eV]	
	6 H ₂ O	12 H ₂ O	6 H ₂ O	12 H ₂ O
mean	−0.89	−1.01	0.42	0.40
min	−1.13	−1.28	0.13	0.12
max	−0.60	−0.48	0.70	0.58
SD	0.14	0.21	0.16	0.15

case of COOH*, the adsorption energy ranges from 0.13 eV to 0.70 eV for six explicit water molecules and from 0.12 eV to 0.58 eV for 12 water molecules.

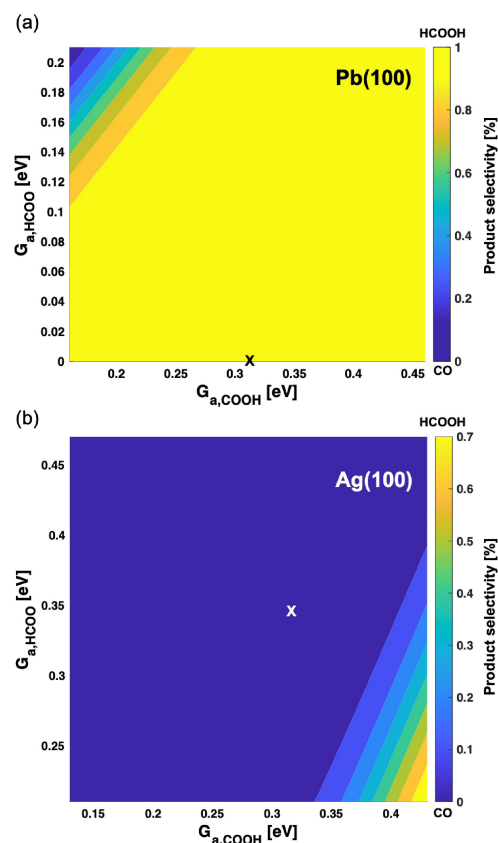
Interestingly, for pure water structures the uncertainty ranges are much lower (as shown in Figure S6 of the Supporting Information), which means that the presence of adsorbates contributes significantly to a greater degree of possible configurations and uncertainty of adsorption energies. Furthermore, the mean adsorption energy of HCOO* for both cases ranges from around −1.01 eV to −0.89 eV, while the mean adsorption energy of COOH* ranges from only 0.40 eV to 0.42 eV, confirming our above observation that HCOO* in solvation tends to change its configuration more frequently leading to more degrees of freedom and ultimately a greater range of adsorption energies. We have also compared adsorption energies of HCOO* at Pb(100) computed with 12 explicit water molecules with an increased sample size of $n = 38$ (Figure S7, Supporting Information). Apart from an increase in the Min-Max range by 0.09 eV, the mean and SD of the HCOO* adsorption energy are comparable to the results of the smaller sample size of $n = 19$.

The results in Table 4 show that adsorption energies of HCOO* and COOH* with 12 explicit H₂O molecules on the Pb(100) surface vary with a SD of 0.21 eV and 0.15 eV, respectively. However, our initial computational predictions of product selectivities discussed in the previous section are based on only one representative HCOO* and one representative COOH* configuration. Therefore, we have conducted a sensitivity analysis of our previous explicit solvation results retrospectively, to bolster the confidence of our initial computational predictions. By varying HCOO* and COOH* adsorption energies on both Pb(100) and Ag(100) surfaces, along with their corresponding SD from Table 5, selectivities towards HCOOH and CO over a range of adsorption energies can be generated. In this context, we make the assumption that altering the adsorption energies, $E_{\text{ads,COOH}^*/\text{HCOO}^*}$ results in an identical change in the activation barrier, $G_{\text{a,COOH}^*/\text{HCOO}^*}$.

Figure 5 illustrates the HCOOH and CO selectivity of CO₂ reduction at both Pb(100) and Ag(100) surfaces over a range of activation barriers for HCOO*, $G_{\text{a,HCOO}^*}$ and COOH*, $G_{\text{a,COOH}^*}$. As shown in Figure 5, the reference case (marked with x) from the section *Reaction energy pathways for CO₂ reduction reaction on Pb(100) and Ag(100) surfaces* gives high selectivity towards CO

Table 5. Statistical mean, minimum (Min), maximum (Max) and standard deviation (SD) of HCOO* adsorption energy, $E_{\text{ads,HCOO}^*}$ and COOH* adsorption energy, $E_{\text{ads,COOH}^*}$ on Pb(100) and Ag(100) surface in the presence of one explicit water layer. A sample size of $n = 19$ was used.

Variables	Pb(100)		Ag(100)	
	$E_{\text{ads,HCOO}^*}$ [eV]	$E_{\text{ads,COOH}^*}$ [eV]	$E_{\text{ads,HCOO}^*}$ [eV]	$E_{\text{ads,COOH}^*}$ [eV]
mean	−1.01	0.40	−0.71	0.35
min	−1.28	0.12	−0.92	0.03
max	−0.48	0.58	−0.50	0.63
SD	0.21	0.15	0.13	0.15

**Figure 5.** Contour graph showing HCOOH and CO product selectivity on (a) Pb(100) surface and (b) Ag(100) surface with varying $G_{\text{a,HCOO}^*}$ and $G_{\text{a,COOH}^*}$. x indicates the reference case that was extracted from Figure 4.

on Ag and high selectivity towards HCOOH on Pb. Varying $G_{\text{a,HCOO}^*}$ and $G_{\text{a,COOH}^*}$ over a range of one SD does not change the initial trend. Only for the extreme cases of $G_{\text{a,COOH}^*} < 0.2$ eV and $G_{\text{a,HCOO}^*} > 0.18$ eV at Pb(100) surface and $G_{\text{a,COOH}^*} > 0.4$ eV and $G_{\text{a,HCOO}^*} < 0.25$ eV at Ag(100) surface we observe a reverse trend. The observation that the HCOOH and CO selectivities within the considered activation energy range largely align with the selectivities observed in the reference case, provides strong support for predictions made in the previous section.

The two important lessons to take away from this section are: (1) it is of utmost importance to provide uncertainty ranges for solvated adsorption energies containing static water structures in order to evaluate the confidence of subsequent

computational predictions with respect to experimental observations and (2) the more explicit water molecules are incorporated in simulations, the bigger is the configurational space of the explicit water molecules, leading to a larger range of possible configurations. Consequently, the greater configurational space results in a higher uncertainty range of adsorption energies. Thus, we must exercise caution when interpreting computational results in explicit solvation environment.

Potential descriptors that affect HCOO* and COOH* adsorption energy in solvation

As shown in the previous section, calculating exact HCOO* and COOH* adsorption energies in solvation environment can be challenging, owing to the large configurational space of the system. While the task of precisely identifying the properties that contribute to the variation in adsorption energies in solvation can become quite complex, we discuss potential descriptors that can affect the adsorption energy of HCOO* in solvation. For this, we have considered five different configurations of HCOO* on the Pb(100) surface in the presence of 12 explicit water molecules generated and optimized using the combined MD/DFT method (as described in Section *Explicit solvation uncertainty analysis of HCOO* and COOH* adsorption energy*). Figure 6 shows the comparison of the five different HCOO*-water configurations based on properties such as total number of H-bonds, number of H-bonds with HCOO*, average HCOO* distance from the Pb(100) surface, the cavitation energy E_{cav} and the adsorbate insertion energy E_{ins} .

While the definitions of total number of H-bonds and number of H-bonds with HCOO* follow common notions, the average HCOO distance from the Pb(100) surface is defined as the vertical distance between the average central plane of the first Pb layer and the average oxygen position of the HCOO* adsorbate. The cavitation energy E_{cav} is defined here as the energy needed for the water structure to reorganize when the adsorbate is present compared to when it is not present and the adsorbate insertion energy E_{ins} is defined as the energy difference between the adsorbate with its surrounding solvation shell compared to the noninteracting adsorbate and the solvation shell.^[20] Graphical definitions of E_{cav} and E_{ins} are provided in Figure S8 of the Supporting Information.

At first sight, the total number of hydrogen bonds in the system correlates well with the magnitude of the adsorption energies of our five representative configurations. The more hydrogen atoms exist in the system, the higher is the adsorption energy of HCOO* in solvated environment. Configuration 1 involves 20 H-bonds with an adsorption energy of -1.37 eV, while configuration 2 has 15 H-bonds with an adsorption energy of only -0.48 eV. However, on a quantitative level, the correlation with the number of H-bonds fails to explain why configurations 3, 4 and 5 have the same adsorption energy with different number of hydrogen bonds. There must exist other descriptors that impact the adsorption energy apart from the number of hydrogen bonds, albeit not as significant.

While the number of hydrogen bonds of HCOO* with its surrounding solvation shell is mostly constant (4 hydrogen bonds) for most of the configurations, we can exclude it from being a potential descriptor. However, the average formate distance from the Pb(100) surface together with the total

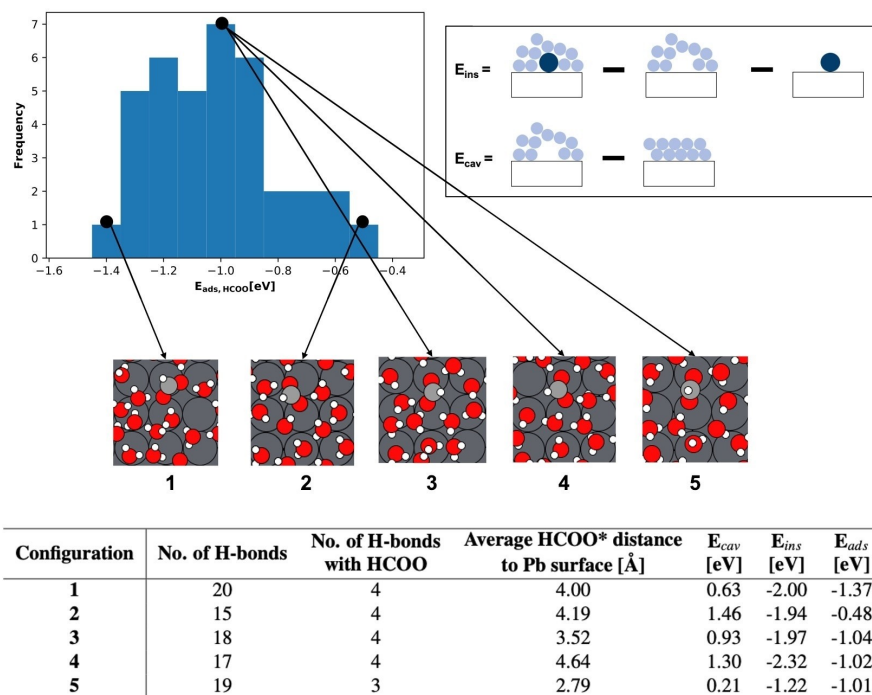


Figure 6. Comparison of five different configurations of HCOO in the presence of 12 explicit water molecules based on number of H-bonds, number of H-bonds with HCOO, average HCOO distance from the Pb(100) surface, E_{cav} and E_{ins} . The configurations are picked out from a sample size of $n = 38$.

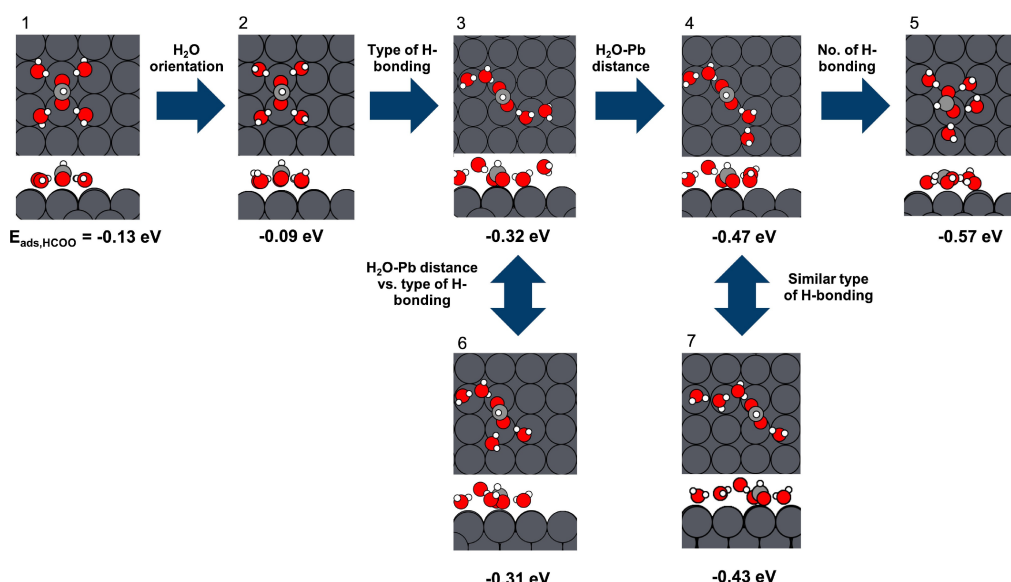


Figure 7. HCOO* adsorption energy comparison of different water configurations for 4 explicit H₂O on the Pb(100) surface.

number of H-bonds from HCOO–H₂O and H₂O–H₂O interactions, are capable of explaining why configurations 3, 4 and 5 have the same adsorption energy with different number of H-bonds. For the three cases, an increasing number of hydrogen bonds is accompanied by a decreasing average distance of formate to the metal surface, which leads to comparable adsorption energies.

For the last two descriptors, E_{ins} and E_{cav} , E_{ins} is not capable of describing the adsorption trend, while E_{cav} can only qualitatively explain the higher adsorption energy with decreasing cavitation energy. Considerations of E_{ins} and E_{cav} as descriptors, as proposed in the existing literature,^[20] fails to properly explain the adsorption trends observed for HCOO* in the presence of 12 explicit water molecules. So far only the total number of hydrogen bonds has shown to exert a significant impact on the HCOO* adsorption energy. It remains, however, difficult to find a global descriptor that captures all effects on the adsorption energy, let alone a system containing 12 explicit water molecules.

Therefore, we have attempted to disentangle different effects that govern the adsorption energy of solvated HCOO* by analyzing HCOO* in the presence of only four explicit molecules, which is equivalent to the number of hydrogen bonds in the first solvation shell of formate. Figure 7 shows the different configurations of formate with four water molecules, starting with a reference configuration 1 and then changing its configurations slightly to observe the impact of different effects such as the number of H-bonds, the type of H-bonding, the water-metal distance as well as the orientation of the explicit water molecules. Configuration 5 has the highest adsorption energy with –0.57 eV, which is 0.44 eV more stable than the reference configuration 1. While the reference configuration consists of only four hydrogen bonds, configuration 5 has five hydrogen bonds leading to the higher adsorption energy. Apart from the total number of hydrogen bonds, the type of

hydrogen bonding also affects the magnitude of the adsorption energy. While both configuration 2 and 3 contain 4 hydrogen bonds, their adsorption energies vary by 0.23 eV, which can be explained by the fact that configuration 3 has two H-bonds stemming from water molecules while the other two stem from formate with its surrounding water molecule. On the other hand, configuration 2 has all its H-bonds stemming from the interaction between formate and its surrounding water molecules, indicating that water-water H-bonding is more stable compared to formate-water H-bonding.

We observe an additional stabilization of the solvated formate adsorption energy as captured in configuration 4 compared to configuration 3, attributed to the reduced water-metal distance. Lastly, the orientation of water molecules has a minor effect on the adsorption energy (configuration 1 vs. configuration 2).

In total, we have assessed four potential descriptors that govern the adsorption energy of solvated HCOO* at the Pb(100) surface. We discovered that there is no single global descriptor that can fully account for the variation in adsorption energy. Instead, a combination of all four descriptors is essential to describe the change in adsorption energy, with the total number of hydrogen bonds per unit cell being the most significant one followed by the type of hydrogen bonding, the water-metal distance and lastly, the orientation of water molecules.

Conclusions

We have performed a systematic study on the role of solvation effects on the CO₂ reduction reaction towards HCOOH and CO at Pb(100) and Ag(100) surfaces. We have demonstrated how the number of explicit water molecules exerts a substantial effect on the adsorption energy of relevant reaction intermedi-

ates. Implicit solvation affects the adsorption energy in a much less pronounced manner than explicit solvation. Using an explicit solvation scheme in combination with microkinetic modeling, we were able to identify CO as the main product at Ag and HCOOH as the main product at Pb, which is in agreement with experimental observations. To the best of our knowledge, this is the first computational demonstration of predicting the main products from CO₂ reduction reaction at both Ag and Pb catalyst, taking into account solvation phenomena.

When it comes to calculating adsorption energies of reaction intermediates in explicit solvation environment, assessment of the uncertainty of computed adsorption energies is a necessary step to evaluate the accuracy of the method. We have attempted to delineate properties affecting the computed adsorption energy of HCOO* on Pb(100) surface. The total number of H-bonds, originating from HCOO–H₂O and H₂O–H₂O interactions, emerged as the main property determining the HCOO* adsorption energy. Other factors such as the type of H-bonding, the adsorbate-metal distance or the orientation of water molecules were found to play a less significant role in this regard.

Overall, this work provides valuable insight into the role of different solvation methods of adsorbates on metal surfaces, and it reveals explicit solvation as a vital effect to be included in the computation of pathways of the CO₂ reduction reaction.

Theoretical Section

DFT calculations

Periodic density functional theory (DFT) calculations were performed for different adsorbates on Pb(100) and Ag(100) surfaces with the PBE exchange correlational functional^[60] using the Quantum-ESPRESSO package.^[61] We used the projector augmented wave (PAW) method for the core electrons.^[62] The plane wave cutoff energy was set to 50 Ry. We applied the atomic simulation environment (ASE) to create 3×3 surfaces represented by five-layer slabs.^[63] The two bottom layers were kept fixed during the geometry optimization, while the other three layers were allowed to relax. In order to avoid undesired interactions between periodically repeated slabs, a 20 Å vacuum space was inserted between them. A Monkhorst–Pack^[64] 4×4×1 k-point grid was used for structure relaxations. The calculated lattice constants of bulk Pb and Ag are 5.03 Å and 4.15 Å, respectively, which are comparable to the measured values of 4.95 Å for Pb^[3] and 4.09 Å for Ag^[65]. Explicit solvation structures were modeled using up to 12 explicit water molecules and implicit solvation calculations were performed with the soft-sphere continuum solvation (SSCS) approach using the Environ software package.^[66,67] During implicit solvation calculations, we assumed a dielectric constant of $\epsilon = 80$ for the bulk solvent value. A hybrid solvation approach was also applied by adding implicit solvation on top of the optimized explicit water configurations.

Adding dispersion corrections, using for instance the D3 dispersion correction scheme of Grimme,^[68,69] can correct for the overstructuring of water molecules in the bulk environment typically seen with the PBE functional.^[70] On the other hand, dispersion effects have a negligible impact on the relative stability, adsorption sites, and adsorption geometries of water adstructures.^[71,72] In

addition, Romeo et al.^[73] have additionally shown that dispersion corrections are generally not significant when water-adsorbate interactions prevail. Therefore, to assess the need of dispersion corrections for our given system, we have incorporated additional calculations that include D3 dispersion corrections with zero damping.

CMD calculations

Classical molecular dynamics (CMD) simulations on the Pb surface were performed with the LAMMPS software package^[74] using 95 explicit water molecules, equivalent to a water density of 1 g L^{−1} for our system size. The interatomic interactions were described by the interface force field (IFF)^[75] and the SPC water model.^[76] The interaction cutoff distance was set to 12 Å and initial water molecule configurations on the Pb(100) surface were obtained by random water molecule placement using the PACKMOL package.^[77] MD simulations were performed under NVT conditions at a temperature of 300 K, with a timestep of 1 fs and a Nose-Hoover thermostat with a temperature damping parameter of 100 fs.

Explicit solvation configuration setup

Regarding the representative configuration used for the case of 1–12 explicit H₂O molecules, we initially generated and conducted geometry optimizations of 5 different random configurations for the case of 1 explicit H₂O molecule. We selected the most energetically stable configuration as the representative structure for the case with 1 explicit H₂O molecule. For the case of 2 explicit water molecules, we used the most energetically stable configuration with 1 explicit H₂O molecule as a basis to generate and optimize 5 further different random configurations. This procedure was repeated until 12 explicit water molecules were added at the Pb(100) surface, which is approximately the amount of water molecules needed to form the first interfacial water layer.^[42] Even though the described water configuration generation procedure does not sample the whole configurational space, this so-called “brute intuition” approach, originally mentioned by Peterson,^[78] to finding local minima configurations follows a simple and reproducible protocol. Hence, we have applied this approach to determine the local minimum configuration of adsorbate-water structures on Pb(100). More details on the initialization of the explicit water structure is given in Figure S9 in the Supporting Information.

Reaction energy calculations

To construct reaction energy diagrams, as shown in Figures 3 and 4, zero-point energy (ZPE) and entropic (TS) corrections are included, which are obtained through vibrational frequency calculations, as shown in Figure S10 in the Supporting Information. The climbing image nudged elastic band (CI-NEB) method^[51] with eight images was utilized to calculate the activation barriers for specific reaction steps.

Microkinetic modeling

In the microkinetic model, the steady state rate equations for the changes of adsorbate coverages in vacuum environment are

$$\frac{d\theta_{\text{HCOO}^*}}{dt} = v_1 - v_2 = 0 \quad (6)$$

$$\frac{d\theta_{\text{COOH}^*}}{dt} = v_3 - v_4 = 0 \quad (7)$$

where θ_{HCOO^*} and θ_{COOH^*} are coverages for HCOO and COOH intermediates. v_i is the reaction rate of the i -th elementary reaction step from Eqs. (1)–(4) and is given by

$$v_1 = k_1 p_{\text{CO}_2} p_{\text{H}_2}^{\frac{1}{2}} \theta_0^2 - k_{-1} \theta_{\text{HCOO}^*} \quad (8)$$

$$v_2 = k_2 \theta_{\text{HCOO}^*} p_{\text{H}_2}^{\frac{1}{2}} \quad (9)$$

$$v_3 = k_3 p_{\text{CO}_2} p_{\text{H}_2}^{\frac{1}{2}} \theta_0^2 - k_{-3} \theta_{\text{COOH}^*} \quad (10)$$

$$v_4 = k_4 \theta_{\text{COOH}^*} p_{\text{H}_2}^{\frac{1}{2}} \quad (11)$$

with $\theta_0 = 1 - 2\theta_{\text{HCOO}^*} - \theta_{\text{COOH}^*}$ being the coverage of free sites, and p_{CO_2} and p_{H_2} being the pressures of CO_2 and H_2 , respectively. We use $p_{\text{CO}_2} = p_{\text{H}_2} = 1$ atm, corresponding to standard conditions. Rate constants, k_{+i} and k_{-i} are calculated from transition-state theory,

$$k_{\pm i} = \frac{k_{\text{B}} T}{h} \exp\left(-\frac{G_{\text{a},\pm i}}{k_{\text{B}} T}\right) \quad (12)$$

where $G_{\text{a},\pm i}$ are activation barriers of step i for the forward and backward reactions obtained from our DFT calculations. θ_{HCOO^*} and θ_{COOH^*} can then be obtained by solving Eqs. (6) and (7).

The selectivities of the two main products CO and HCOOH can then be calculated by Equations (13) and (14).

$$s_{\text{CO}} = \frac{v_4}{v_2 + v_4} \quad (13)$$

$$s_{\text{HCOOH}} = \frac{v_2}{v_2 + v_4} \quad (14)$$

Supporting Information

The authors have cited additional references within the Supporting Information.^[79]

Acknowledgements

We acknowledge the computational resources on RWTH Aachen University and Forschungszentrum Jülich provided by JARA-CSD. This study was conducted as part of the Helmholtz program on Materials and Technologies for the Energy Transition. We are grateful to Jun Huang and Mohammad Javad Eslamibidgoli for the helpful discussions. We are grateful to Piotr M. Kowalski for feedback on the manuscript. Open Access funding enabled and organized by Projekt DEAL.

Conflict of Interests

The authors declare no conflict of interest.

Data Availability Statement

The data that support the findings of this study are available from the corresponding author upon reasonable request.

Keywords: ab initio calculations · CO_2 reduction · electrochemistry · metal-water interface · solvent effects

- [1] M. Neurock, S. A. Wasileski, D. Mei, *Chem. Eng. Sci.* **2004**, *59*, 4703.
- [2] M. García-Ratés, R. García-Muelas, N. López, *J. Phys. Chem. C* **2017**, *121*, 13803.
- [3] M. Fan, M. J. Eslamibidgoli, X. Zhu, S. Garbarino, A. C. Tavares, M. Eikerling, D. Guay, *ACS Catal.* **2020**, *10*, 10726.
- [4] X. Nie, W. Luo, M. J. Janik, A. Asthagiri, *J. Catal.* **2014**, *312*, 108.
- [5] S. N. Steinmann, P. Sautet, C. Michel, *Phys. Chem. Chem. Phys.* **2016**, *18*, 31850.
- [6] F. Calle-Vallejo, R. F. de Morais, F. Illas, D. Loffreda, P. Sautet, *J. Phys. Chem. C* **2019**, *123*, 5578.
- [7] H. H. Heenen, J. A. Gauthier, H. H. Kristoffersen, T. Ludwig, K. Chan, *J. Chem. Phys.* **2020**, *152*, 144703.
- [8] S. K. Iyemperumal, N. A. Deskins, *ChemPhysChem* **2017**, *18*, 2171.
- [9] S. Sakong, A. Groß, *Phys. Chem. Chem. Phys.* **2020**, *22*, 10431.
- [10] P. Clabaut, B. Schweitzer, A. W. Götz, C. Michel, S. N. Steinmann, *J. Chem. Theory Comput.* **2020**, *16*, 6539.
- [11] A. Rendón-Calle, S. Builes, F. Calle-Vallejo, *Appl. Catal. B* **2020**, *276*, 119147.
- [12] A. Bagger, L. Arnarson, M. H. Hansen, E. Spohr, J. Rossmeisl, *J. Am. Chem. Soc.* **2019**, *141*, 1506.
- [13] M. Valter, B. Wickman, A. Hellman, *J. Phys. Chem. C* **2021**, *125*, 1355.
- [14] Y. Mei, N. A. Deskins, *Phys. Chem. Chem. Phys.* **2021**, *23*, 16180.
- [15] M. Zare, M. Saleheen, S. K. Kundu, A. Heyden, *Commun. Chem.* **2020**, *3*, 187.
- [16] J. Santatiwongchai, K. Faungnawakij, P. Hirunsit, *ACS Catal.* **2021**, *11*, 9688.
- [17] G. Di Liberto, L. Giordano, *Electrochem. Sci. Adv.* **2023**, e2100204.
- [18] S. Schnur, A. Groß, *New J. Phys.* **2009**, *11*, 125003.
- [19] Y. Gohda, S. Schnur, A. Groß, *Faraday Discuss.* **2009**, *140*, 233.
- [20] T. Ludwig, J. A. Gauthier, K. S. Brown, S. Ringe, J. K. Nørskov, K. Chan, *J. Phys. Chem. C* **2019**, *123*, 5999.
- [21] G. Cicero, A. Calzolari, S. Corni, A. Catellani, *J. Phys. Chem. Lett.* **2011**, *2*, 2582.
- [22] O. Cheong, M. H. Eikerling, P. M. Kowalski, *Appl. Surf. Sci.* **2022**, *589*, 152838.
- [23] S. N. Steinmann, R. Ferreira De Morais, A. W. Götz, P. Fleurat-Lessard, M. Iannuzzi, P. Sautet, C. Michel, *J. Chem. Theory Comput.* **2018**, *14*, 3238.
- [24] A. Berg, C. Peter, K. Johnston, *J. Chem. Theory Comput.* **2017**, *13*, 5610.
- [25] Y. Hori, *Electrochemical CO_2 Reduction on Metal Electrodes, in Modern Aspects of Electrochemistry*, vol. 42, pages 89–189, Springer New York **2008**.
- [26] S. Nitopi, E. Bertheussen, S. B. Scott, X. Liu, A. K. Engstfeld, S. Horch, B. Seger, I. E. L. Stephens, K. Chan, C. Hahn, J. K. Nørskov, T. F. Jaramillo, I. Chorkendorff, *Chem. Rev.* **2019**, *119*, 7610.
- [27] C. H. Lee, M. W. Kanan, *ACS Catal.* **2015**, *5*, 465.
- [28] C. Cui, H. Wang, X. Zhu, J. Han, Q. Ge, *Sci. China Chem.* **2015**, *58*, 607.
- [29] A. K. Singh, S. Singh, A. Kumar, *Catal. Sci. Technol.* **2016**, *6*, 12.
- [30] J. Klankermayer, S. Wesselbaum, K. Beydoun, W. Leitner, *Angew. Chem. Int. Ed.* **2016**, *55*, 7296.
- [31] J. Hietala, A. Vuori, P. Johnsson, I. Pollari, W. Reutemann, H. Kieczka, Formic Acid, in *Ullmann's Encyclopedia of Industrial Chemistry*, pages 1–22, Wiley-VCH Verlag GmbH & Co. KGaA **2016**.
- [32] H. Papp, M. Baerns, in *New Trends in Coactivation, volume 64 of Studies in Surface Science and Catalysis*, Chapter 10 Industrial Application of CO Chemistry for The Production of Specialty Chemicals, pages 430–461, Elsevier **1991**.
- [33] N. J. Firet, W. A. Smith, *ACS Catal.* **2017**, *7*, 606.
- [34] J. T. Feaster, C. Shi, E. R. Cave, T. Hatsukade, D. N. Abram, K. P. Kuhl, C. Hahn, J. K. Nørskov, T. F. Jaramillo, *ACS Catal.* **2017**, *7*, 4822.
- [35] J. S. Yoo, R. Christensen, T. Vegge, J. K. Nørskov, F. Studt, *ChemSusChem* **2016**, *9*, 358.
- [36] A. Bagger, W. Ju, A. S. Varela, P. Strasser, J. Rossmeisl, *ChemPhysChem* **2017**, *18*, 3266.
- [37] J. Hussain, H. Jónsson, E. Skúlason, *ACS Catal.* **2018**, *8*, 5240.

- [38] A. R. T. Morrison, M. Ramdin, L. J. P. van der Broeke, W. de Jong, T. J. H. Vlugt, R. Kortlever, *J. Phys. Chem. C* **2022**, 126, 11927.
- [39] D. Bohra, I. Ledezma-Yanez, G. Li, W. De Jong, E. A. Pidko, W. A. Smith, *Angew. Chem. Int. Ed.* **2019**, 58, 1345.
- [40] X.-G. Zhang, X. Jin, D.-Y. Wu, Z.-Q. Tian, *J. Phys. Chem. C* **2018**, 122, 25447.
- [41] A. Seifitokaldani, C. M. Gabardo, T. Burdyny, C.-T. Dinh, J. P. Edwards, M. G. Kibria, O. S. Bushuyev, S. O. Kelley, D. Sinton, E. H. Sargent, *J. Am. Chem. Soc.* **2018**, 140, 3833.
- [42] X. Lin, F. Evers, A. Groß, *Beilstein J. Nanotechnol.* **2016**, 7, 533.
- [43] J. K. Nørskov, J. Rossmeisl, A. Logadottir, L. Lindqvist, J. R. Kitchin, T. Bligaard, H. Jónsson, *J. Phys. Chem. B* **2004**, 108, 17886.
- [44] P. M. Kowalski, T. Bornhake, O. Cheong, N. Dohrmann, A. L. Koch Liston, S. K. Potts, A. Shad, R. Tesch, Y.-Y. Ting, *Front. Energy Res.* **2023**, 10, 1096190.
- [45] G. Kresse, J. Hafner, *Phys. Rev. B* **1993**, 47, 558.
- [46] G. Kresse, J. Furthmüller, *Comput. Mater. Sci.* **1996**, 6, 15.
- [47] G. Kresse, J. Furthmüller, *Phys. Rev. B* **1996**, 54, 11169.
- [48] K. Mathew, V. S. C. Kolluru, S. Mula, S. N. Steinmann, R. G. Hennig, *J. Chem. Phys.* **2019**, 151, 234101.
- [49] K. Mathew, R. Sundararaman, K. Letchworth-Weaver, T. A. Arias, R. G. Hennig, *J. Chem. Phys.* **2014**, 140, 084106.
- [50] X. Lin, A. Shao, M. Hua, X. Tian, *Phys. Chem. Chem. Phys.* **2022**, 24, 6803.
- [51] G. Henkelman, B. Uberuaga, H. Jonsson, *J. Chem. Phys.* **2000**, 113, 9901.
- [52] M. Van den Bossche, C. Rose-Petruck, H. Jónsson, *J. Phys. Chem. C* **2021**, 125, 13802.
- [53] J. A. Gauthier, M. Fields, M. Bajdich, L. D. Chen, R. B. Sandberg, K. Chan, J. K. Nørskov, *J. Phys. Chem. C* **2019**, 123, 29278.
- [54] H. Noda, S. Ikeda, Y. Oda, K. Imai, M. Maeda, K. Ito, *BCSJ* **1990**, 63, 2459.
- [55] T. Hatsukade, K. P. Kuhl, E. R. Cave, D. N. Abram, T. F. Jaramillo, *Phys. Chem. Chem. Phys.* **2014**, 16, 13814.
- [56] X. Zhu, J. Huang, M. Eikerling, *ACS Catal.* **2021**, 11, 14521.
- [57] J. Huang, X. Zhu, M. Eikerling, *Electrochim. Acta* **2021**, 393, 139019.
- [58] X. Zhu, J. Huang, M. Eikerling, *JACS Au* **2023**, 3, 1052.
- [59] X. Zhang, R. S. DeFever, S. Sarupria, R. B. Getman, *J. Chem. Inf. Model.* **2019**, 59, 2190.
- [60] J. P. Perdew, K. Burke, M. Ernzerhof, *Phys. Rev. Lett.* **1996**, 77, 3865.
- [61] P. Giannozzi, S. Baroni, N. Bonini, M. Calandra, R. Car, C. Cavazzoni, D. Ceresoli, G. L. Chiarotti, M. Cococcioni, I. Dabo, A. D. Corso, S. de Gironcoli, S. Fabris, G. Fratesi, R. Gebauer, U. Gerstmann, C. Gougousis, A. Kokalj, M. Lazzeri, L. Martin-Samos, N. Marzari, F. Mauri, R. Mazzarello, S. Paolini, A. Pasquarello, L. Paulatto, C. Sbraccia, S. Scandolo, G. Sclauzero, A. P. Seitsonen, A. Smogunov, P. Umari, R. M. Wentzcovitch, *J. Phys. Condens. Matter* **2009**, 21, 395502.
- [62] P. E. Blöchl, *Phys. Rev. B* **1994**, 50, 17953.
- [63] A. Hjorth Larsen, J. Jørgen Mortensen, J. Blomqvist, I. E. Castelli, R. Christensen, M. Dułak, J. Friis, M. N. Groves, B. Hammer, C. Hargus, E. D. Hermes, P. C. Jennings, P. Bjerre Jensen, J. Kermode, J. R. Kitchin, E. Leonhard Kolsbjerg, J. Kubal, K. Kaasbjerg, S. Lysgaard, J. Bergmann Maronsson, T. Maxson, T. Olsen, L. Pastewka, A. Peterson, C. Rostgaard, J. Schiøtz, O. Schütt, M. Strange, K. S. Thygesen, T. Vegge, L. Vilhelmsen, M. Walter, Z. Zeng, K. W. Jacobsen, *J. Phys. Condens. Matter* **2017**, 29, 273002.
- [64] H. J. Monkhorst, J. D. Pack, *Phys. Rev. B* **1976**, 13, 5188.
- [65] I. Shyjumon, M. Gopinadhan, O. Ivanova, M. Quaas, H. Wulff, C. A. Helm, R. Hippler, *Eur. Phys. J. D* **2006**, 37, 409.
- [66] O. Andreussi, I. Dabo, N. Marzari, *J. Chem. Phys.* **2012**, 136, 064102.
- [67] P. Giannozzi, O. Andreussi, T. Brumme, O. Bunau, M. B. Nardelli, M. Calandra, R. Car, C. Cavazzoni, D. Ceresoli, M. Cococcioni, N. Colonna, I. Carnimeo, A. D. Corso, S. d. Gironcoli, P. Delugas, R. A. DiStasio, A. Ferretti, A. Floris, G. Fratesi, G. Fugallo, R. Gebauer, U. Gerstmann, F. Giustino, T. Gorni, J. Jia, M. Kawamura, H.-Y. Ko, A. Kokalj, E. Küçükbenli, M. Lazzeri, M. Marsili, N. Marzari, F. Mauri, N. L. Nguyen, H.-V. Nguyen, A. Otero-de-la Roza, L. Paulatto, S. Poncè, D. Rocca, R. Sabatini, B. Santra, M. Schlipf, A. P. Seitsonen, A. Smogunov, I. Timrov, T. Thonhauser, P. Umari, N. Vast, X. Wu, S. Baroni, *J. Phys. Condens. Matter* **2017**, 29, 465901.
- [68] S. Grimme, *WIREs Comput. Mol. Sci.* **2011**, 1, 211.
- [69] S. Grimme, J. Antony, S. Ehrlich, H. Krieg, *J. Chem. Phys.* **2010**, 132, 154104.
- [70] J. VandeVondele, F. Mohamed, M. Krack, J. Hutter, M. Sprik, M. Parrinello, *J. Chem. Phys.* **2005**, 122, 014515.
- [71] J. Carrasco, J. Klimeš, A. Michaelides, *J. Chem. Phys.* **2013**, 138, 024708.
- [72] H. Chen, M. A. Blatnik, C. L. Ritterhoff, I. Sokolović, F. Mirabella, G. Franceschi, M. Riva, M. Schmid, J. Čechal, B. Meyer, U. Diebold, M. Wagner, *ACS Nano* **2022**, 16, 21163.
- [73] E. Romeo, F. Illas, F. Calle-Vallejo, *J. Phys. Chem. C* **2023**, 127, 10134.
- [74] S. Plimpton, *J. Comput. Phys.* **1995**, 117, 1.
- [75] H. Heinz, T.-J. Lin, R. Kishore Mishra, F. S. Emami, *Langmuir* **2013**, 29, 1754.
- [76] H. J. C. Berendsen, J. R. Grigera, T. P. Straatsma, *J. Phys. Chem.* **1987**, 91, 6269.
- [77] L. Martínez, R. Andrade, E. G. Birgin, J. M. Martínez, *J. Comput. Chem.* **2009**, 30, 2157.
- [78] A. A. Peterson, *Top. Catal.* **2014**, 57, 40.
- [79] P. Hirunsit, *J. Phys. Chem. C* **2013**, 117, 8262.

Manuscript received: June 20, 2023

Revised manuscript received: August 3, 2023

Accepted manuscript online: August 4, 2023

Version of record online: August 24, 2023